Disentangling Heat and Moisture Effects on Biopolymer Mechanics

Chi Zhang, Ali Shomali, Robert Guyer, Sinan Keten, Benoit Coasne, Dominique Derome, Jan Carmeliet

Disentangling Heat and Moisture Effects on Biopolymer Mechanics

Chi Zhang[†‡*], *Ali Shomali*[†], *Robert Guyer*[※], *Sinan Keten*[§], *Benoit Coasne*[ǁ], *Dominique Derome*[‡], *Jan Carmeliet*[†]

[†]Chair of Building Physics, Department of Mechanical and Process Engineering, ETH Zurich, 8093, Zurich, Switzerland

[‡]Laboratory for Multiscale Studies in Building Physics, Swiss Federal Laboratories for Materials Science and Technology, Ueberlandstrasse 129, 8600, Duebendorf, Switzerland

[※]Department of Physics, University of Nevada, Reno, 1664 N. Virginia Street, Reno, NV, 89557, United States

[§]Department of Civil and Environmental Engineering, Northwestern University, 2145 Sheridan Road, Evanston, Illinois, 60208-3109, United States

[ǁ]Univ. Grenoble Alpes, CNRS, LIPhy, 38000 Grenoble, France

Abstract

Heat and moisture are known to have important mechanical effects on polymers such as hygric swelling, thermal expansion and mechanical weakening. A common approach when investigating such effects is to assume the effects of heat and moisture to be similar – the so-called time-temperature-moisture superposition. Through molecular dynamics simulation, this study evaluates the extent of the similarity of the effects of moisture and heat on the hygric swelling, thermal expansion and mechanical weakening of a biopolymer: an uncondensed type of lignin, one of the most abundant polymers in the plant regime. We introduce as a microscopic metric the local stiffness ($T/\langle u^2 \rangle$, temperature divided by the amplitude of segmental motion $\langle u^2 \rangle$), to analyze the mechanisms of mechanical effects of heat and moisture. The local stiffness of polymer skeleton and the overall stiffness of the composite material are shown to be strongly correlated, with a Pearson correlation coefficient of 0.96. Under the assumptions of harmonic vibration and isotropy, an explicit equation relating bulk moduli and the local stiffness can be derived, and the theoretically predicted moduli are in good agreement with measurement. The thermal expansion and weakening are shown to be related to each other and both dependent on the local stiffness. The analysis of the potential energy further points out that heating weakens both primary and secondary bonds of the polymer skeleton, while hydration only affects the secondary bonds. This major difference is thought to be the origin of the different impacts of heat and moisture on biopolymer mechanics, offering a different view of the time-temperature-moisture superposition principle.

1 Introduction

The influence of heat and moisture on the mechanics of polymers is a fundamental issue with particular relevance to many industrial applications such as textiles, packaging, food science, and building materials. The systematic understanding of the coupled physics of moisture and heat is important for effective utilization of many natural and synthetic polymeric materials.

For a large variety of polymers establish the time-temperature superposition principle (TTSP), also named the thermo-rheologically simple postulate, meaning that an increment in temperature is equivalent to an increment of time of observation. The shapes of the elastic moduli vs. time curves under different temperature conditions assemble each other, except for a horizontal shift. In fact, in addition to temperature, a number of other shifting factors are known, such as moisture content, diluent concentration, blend ratios and etc. Varying jointly moisture content and temperature creates a "doubly shifted" master curve, based on which a number of experimental reports proposed the so-called time-temperature-moisture superposition principle (TTMSP) of polymers.[1–7] This master curve also suggests that the influence of heat and moisture can be treated using mathematical forms similar to the Williams-Landel-Ferry (WLF) equation,[1,8,9] though it is reported that the TTMSP may not hold for low moisture content.[10] The moisture content is sometimes referred to as "apparent temperature", where an increment in moisture content is taken as an equivalent of the rise of temperature.[11] The current demonstration of the validity of TTMSP is based on macroscopic and phenomenological observations but lacks observations of the mechanisms at play at microscales. The similar effects of heat and moisture on polymers elastic behavior have yet to be analyzed and their mechanisms at origin elucidated.

In this paper, we discuss the heat and moisture effects in terms of their similarities and also their differences, the latter a topic rarely touched in literature. Molecular dynamics (MD), a simulation method widely used in bio-physics or materials science, is chosen as the main tool of

investigation. Applying proper force field parameters and potential equations, MD allows capturing the trajectories of atoms at femtosecond time resolution giving microscopic information. Based on such microscopic movements of atoms, macroscopic variables such as temperature, pressure, enthalpy can be harvested using statistical thermodynamics, making MD a powerful tool for investigating physical and mechanical aspects. Here we focus on the instantaneous elastic response of a model polymeric material.

This study uses the uncondensed type of lignin (uLGN) as a prototypical polymer, lignin being one of the most abundant biopolymers on Earth. We recall that uncondensed lignin is a linear polymer, not to be confused with condensed lignin also present in plants, which is randomly cross-polymerized. uLGN is known to be moderately hydrophilic thus serving as a complement to frequently studied hydrophilic polymeric materials, such as nylon (polyamide),[12] polyvinyl acetate (PVAc)[1] and polyvinyl alcohol (PVA)[4]. There have been several MD studies focused on various properties of lignin. Petridis et al. study the temperature-dependent structure and dynamics of randomly branched lignin, i.e. condensed type of lignin, and observed that temperature rise enhances dynamics and transits the polymer from compact to extended conformations.[13,14] Vural et al. combine MD and experiments, namely neutron scattering and dielectric spectroscopy, and found that a hysteresis exists where lignin shows faster dynamics and a larger size at a given temperature when being cooled than being heated.[15] Buehler et al. investigated the influence of lignin structure on the deformation of wood cell walls.[16] Beste et al. used the ReaxFF force field to investigate the thermal decomposition in oxygen environment of the most common linkages in softwood.[17] Despite these works, there is a lack of comprehensive study of the mechanics of lignin under various temperatures and moisture contents. In particular,

a better understanding of the microscopic mechanisms of the combined impact of heat and moisture could help to improve the delignification process, a common pretreatment of biomass.

There are few papers discussing the combined influence of heat and moisture on the mechanical behavior of polymers using MD. Xin and Han show that both heat and moisture water reduces the mechanical properties of the cross-linked epoxy.[18] Vural et al. find a similar effect of either heat or moisture on polymer segmental relaxation.[19] Suarez-Martinez et al. show that both temperature and water affect the dynamics of the polyelectrolyte chain in a similar way supporting the time–water–temperature superposition principles.[7] However, the occurrence of a difference in the moisture and heat influence on the mechanical properties of a polymer, be it lignin, as yet to be investigated with MD.

Our study aims at understanding the microscopic mechanisms of hygric swelling, thermal expansion and mechanical weakening under hygric and thermal loadings. To perform this study we determine the local stiffness of the polymer skeleton and the adsorbed water at the microscale. Strikingly simple equations relating the amplitude of segmental motion, sometimes referred to as the Debye-Waller factor, and the macroscopic elastic moduli are derived for the first time. We explain the similarities and differences between the effects of heat and moisture on fundamental aspects of a polymer, namely lignin, taking into account the molecular mobility and energetics. The proposed method offers a way to relate microscopic quantities to macroscopic observables. The results, and the proposed methodology, might be important to various applications such as biofuel production, paper making and hygro-thermo-treatment of wood.

2 Modeling methods

2.1 Preparation of the hydrated polymeric system

Uncondensed lignin (uLGN) of softwood consists of linear chain of β-O-C4 linked coniferyl units, as shown in Figure 1. The C2, C5 and C6 positions of the monomer are free of substitution while the C3 position is substituted with a methoxyl group.[20] We note that the exact structure of lignins in plants is still ongoing investigation due to its complex nature. The polymer uLGN is understood to be of rather linear type, but we note a lack of experimental characterization of pure uLGN material, caused by the difficulties of its extraction without chemical alteration. This computational study of uLGN serves as a helpful complement. The molecular model here contains five chains with a degree of polymerization 100. The degree of polymerization corresponds to experimental reports.[21]

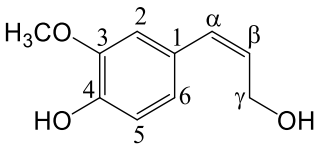

Figure 1. Chemical structure of the monomer of uncondensed lignin, coniferyl unit.

The initial chemical structure is built in Material Studio 8.0. For MD simulations, Gromacs 5.0[22] software and Gromos 53a6[23] force field are applied. The Gromos 53a6 force field is chosen because of its unique feature that it is based primarily on reproducing the free enthalpies of hydration and apolar solvation for a range of compounds, which fits the investigations about biomolecule hydration, solvation and association.[23] The automated topology builder (ATB) server was used to carry out the parameterization and the primary geometry optimization.[24–26] The single chains of uLGN are energy minimized. Then, five relaxed chains are placed in one simulation box with full periodic boundary conditions. The system is further relaxed for 20 ns in the isothermal-isobaric ensemble (NPT) using a Nose-Hoover thermostat and a Parrinello-Rahman barostat with temperature and pressure being 300 K and 0 Pa, respectively. The equilibrated system attains a density of 1.33 g/cm^3, which is in accordance with the experimental

result of 1.36 g/cm^3.[27] The Herman's orientation function of the equilibrated structure has a value of 0±0.02 verifying that the simulated material is isotropic. The hydroxyl groups of lignin are evenly distributed in space, meaning that no hydrophobic or hydrophilic pores are formed. All production simulations are carried out under NPT ensemble. In most simulations, the pressure is set to 0 bar, except for the bulk modulus measurements where the system is tested under a specific mechanical loading. The cut-off distance of both Coulombic and van der Waals interactions is set to 1 nm and the long-range Coulombic interactions are calculated by particle mesh Ewald summation. The covalent bonds with hydrogen atoms are constrained with the LINCS algorithm. The time step of integration is 1 fs.

Water molecules are introduced in the system through the random insertion of the single point charge (SPC) model of water, followed by energy minimization and 10 ps of equilibration. The Gromos force field is designed to work with SPC water model. This study focuses on the thermodynamic equilibrium state without the consideration of water diffusion process. The SPC model predicts well the density, heat of vaporization and isothermal compressibility of pure water. However, we note that this model yields a relatively larger value for the thermal expansion coefficient (TEC) than what is measured in experiments.[28] To reach the equilibrated state with less computational cost, the water molecules are initially inserted into random locations and the following equilibration steps allow attaining thermodynamically favored locations. For each moisture level, an extra 20 ns of equilibration is applied. The distribution of water molecules, quantified by the radial distribution function of the oxygen atoms of water, is seen to remain stable after 10 ns, meaning that 20 ns of equilibration time is more than sufficient to reach equilibrium statistically. The polymer carbon atoms radial distribution functions are also

checked in a similar way. In fact, extended simulations as long as 1000 ns are carried out and give similar radial distribution function results as the 20 ns results.

The studied moisture content, reported in mass of water per mass of dry polymer, and the temperature range between 0~30%, with an increment of 4%, and 283~373 K, with an increment of 10 K respectively. We note that these ranges are broader than the ranges of common ambient conditions of wood usage in order to allow a more in-depth investigation. We note that, in the temperature range of investigation, no major change of chemical or physical properties, such as pyrolysis of polymer and phase change of water, occurs. The pyrolysis temperature of lignin (~600 K)[29] is much higher than the maximum temperature studied here. Water molecules confined in porous media have a lower freezing point (<273 K)[30] and higher boiling point (>373 K)[31] than bulk water due to the Gibbs-Thomson effect. This ensures that, in this work, water molecules do not experience phase changes, i.e. freezing or evaporation.

Three repetition systems are prepared following the same modeling process above. They differ by their polymer orientations and initial water insertion locations. All the repetition systems are then tested under the same protocol described below, and the obtained results are averaged with standard deviations indicated.

2.2 Evaluation of the free strain due to changes in moisture content and temperature

The volume of the system, denoted as $V(m,T)$, is measured as the time average volume over a 0.5 ns production run that followed a 1.5 ns equilibration run in the NPT ensemble (P = 0 Pa). The volume is measured under a series of different moisture content and temperature conditions allowing deforming freely. The system reaches its stable state within the first 0.1 ns of the equilibration run. The volumetric strain $\epsilon_V(m,T)$ due to changes in moisture content and temperature is defined as relative difference with respect to the volume at m = 0% and T = 283 K:

$$\epsilon_V(m,T) = \frac{V(m,T) - V(0\%, 283\ \mathrm{K})}{V(0\%, 283\ \mathrm{K})} \quad (1)$$

We refer to this volumetric strain as swelling strain when the moisture content is increased, or as thermal expansion strain when the temperature is increased. In general, we will refer to the volumetric strain as free strain.

2.3 Evaluation of the bulk modulus

The system is equilibrated in NPT (P = 0 bar) for 20 ns to obtain the equilibrium volume $V(m,T)$ in the free stress state. Then equal pressure on x, y and z directions is applied, where the system is simulated in NPT ($P = \sigma$ = 500 bar) for 2 ns to obtain the equilibrium volume in the loaded state $V^{\sigma}(m,T)$. The system equilibrium is reached within the first 0.1 ns of the run, which is much shorter than the total relaxation time given to the system of ~2 ns. The bulk modulus is expressed as:[32]

$$K(m,T) = -V\frac{\partial \sigma}{\partial V} = \sigma \left| \frac{V(m,T)}{V^{\sigma}(m,T) - V(m,T)} \right| \quad (2)$$

The load value σ is chosen to be 500 bar, which is large enough to suppress sufficiently the fluctuation of system volume, and the resulting strain ranges from 2% to 4%.

2.4 Density of the polymer-polymer hydrogen bonds

The criteria for hydrogen bond are defined by the configuration of the donor-hydrogen-acceptor triplet:

$$r \leq 0.35\ nm \text{ and } \alpha \leq 30° \quad (3)$$

where r is the distance between the donor oxygen atom and the acceptor oxygen atom, and α is the angle of acceptor oxygen atom – donor oxygen atom – donor hydrogen atom. The interoxygen distance criterion of 0.35 nm refers to the first minimum of the radial distribution function of SPC water.[33,34] The angle of 30° is approximately the amplitude of vibrations that

191 break hydrogen bonds.[35] In this paper, we only discuss polymer-polymer hydrogen bonds. The
192 number of hydrogen bonds is normalized by the volume at m = 0% and T = 283 K, to eliminate
193 its size dependency, resulting in a Lagrangian density of polymer-polymer hydrogen bonds with
194 a unit of nm^{-3}.

195 2.5 Evaluation of the local stiffness $T/\langle u^2 \rangle$

196 In this paper, we use the local stiffness as a metric at the microscopic scale. The local stiffness
197 is defined as the quotient of temperature T and the $\langle u^2 \rangle$ factor. The $\langle u^2 \rangle$ factor indicates the
198 average displacement of atoms at picosecond time scales and is generally assumed to be related
199 to the mechanical properties, i.e. an inverse proportionality is frequently assumed between the
200 $\langle u^2 \rangle$ factor and the local elastic properties, e.g. high-frequency modulus G_∞,[36] derived on the
201 basis of simple Maxwell model of liquids.[37] The $\langle u^2 \rangle$ is also referred to as the Debye-Waller
202 factor,[38,39] a property of material that can be measured by neutron scattering experiments[40] and
203 molecular simulations.[41] On the molecular level, a chain segment displaces itself within a
204 temporary cage formed by its surrounding segments. The MSD of the chain segment keeps
205 increasing until the movement of the segment is restrained by the boundary of the cage and
206 bounces back. A plateau in the MSD-time plot emerges when such rebound happens, where the
207 corresponding time scale is called the caging time and the corresponding MSD, $\langle u^2 \rangle$, indicates
208 the size of the molecular cage. Beyond the caging time, the chain segments will show diffusive
209 behavior and escape from the cage.

210 If we assume that the chain segment is confined to its equilibrium location by a harmonic
211 spring, the energy of the chain segment movement can be expressed as $k\langle u^2 \rangle$, where k stands for
212 an assumed local spring constant. In this paper, each monomer is taken as a polymer segment
213 and the MSD of its center of mass is measured. Comparing with the MSD of single atoms, the

MSD of the center of mass of the monomer eliminates the contribution of rotation of this monomer to MSD. Within the moisture content and temperature ranges of investigation, the MSD of uLGN polymer plateaus at ~10 ps, due to the confinement of the cage formed by the surrounding atoms of the chain segment. Similar to Xia et al.[41] the $\langle u^2 \rangle$ factor in this study is defined as the average mean square displacement (MSD) of polymer segments at 10 ps, the caging time of uLGN. The $\langle u^2 \rangle$ factor for water is measured similarly, by assessing the average MSD of the center of mass of water molecules.

3 Results and discussion

3.1 Macroscopic results: heat and moisture-induced free strain and mechanical weakening

Figure 2a shows the free strain as a function of both temperature and moisture content, using a green to yellow scale in addition to contour lines. As moisture content and temperature increases, the free strain increases from 0 at T=283 K and m=0 %, to more than 0.4 at T=373 K and m=30 %.

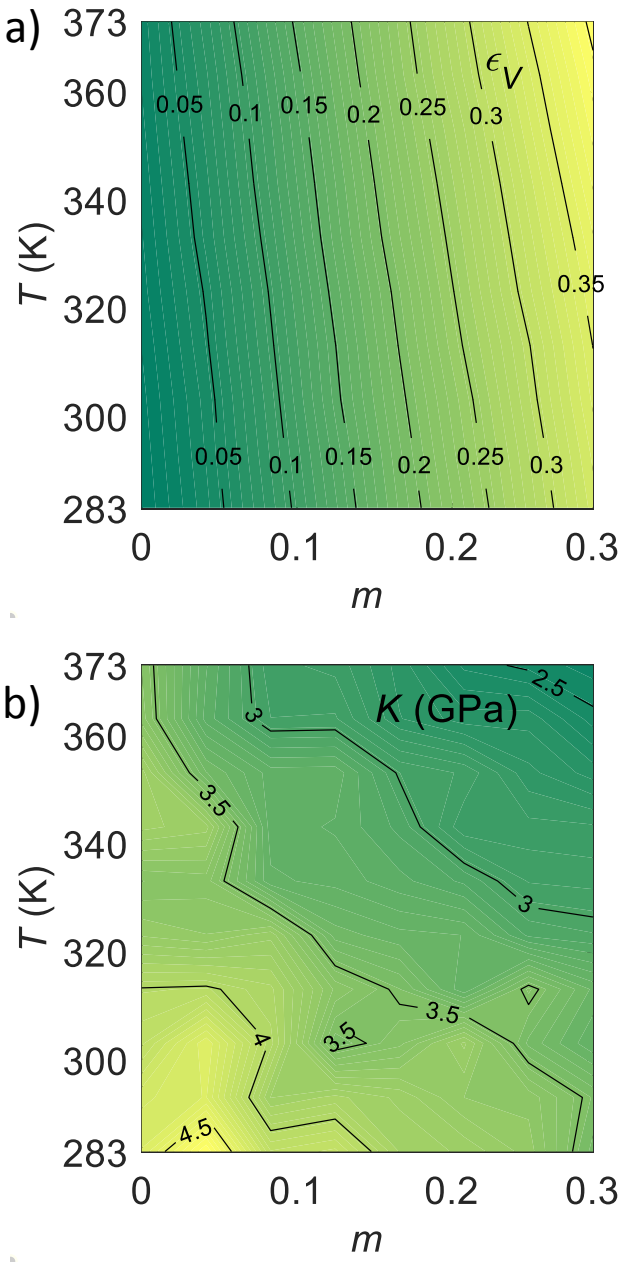

227

228 **Figure 2. a**) Free strain as a function of temperature and moisture content. **b**) Bulk modulus as a

229 function of temperature and moisture content, contour line units are in GPa.

230 The bulk modulus of uLGN as a function of temperature and moisture content is shown in

231 Figure 2b. The higher moduli are denoted by yellow and the lower by green color. As

232 temperature and moisture content increases, the bulk modulus decreases from more than 4.5 GPa

to less than 2.5 GPa indicating a mechanical weakening of the material. Due to scattering, the contour lines are not as smooth as those for the free strain shown in Figure 2a. The rather diagonal lines indicate that the increase of temperature and moisture content both induce weakening.

3.2 Microscopic results: weakening and straining explained by local stiffness $T/\langle u^2 \rangle$

Figure 3 gives the local stiffness $T/\langle u^2 \rangle$ of polymer skeleton and water as a function of temperature and moisture content, respectively.

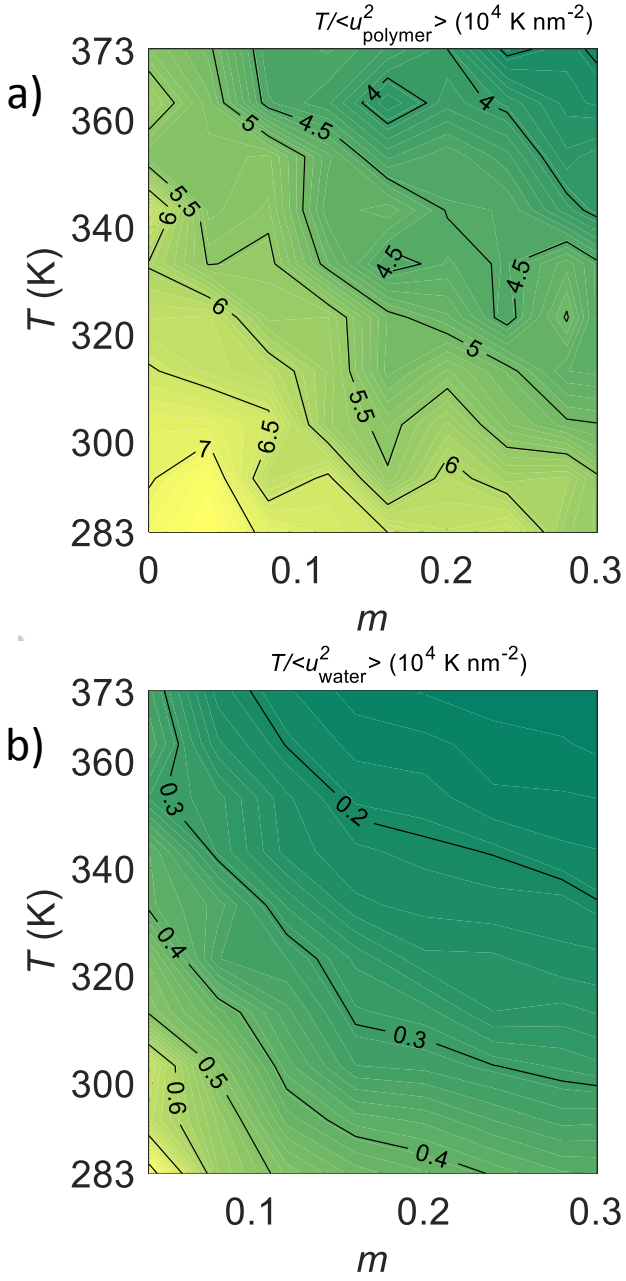

240

241 **Figure 3**. **a**) Local stiffness $T/\langle u^2 \rangle$ of the polymer skeleton as a function of moisture content m
242 and temperature T. **b**) Local stiffness $T/\langle u^2 \rangle$ of water as a function of moisture content m and
243 temperature T. The unit of the contour lines is 10^4 K nm^{-2}.

244 As shown in Figure 3, $T/\langle u^2 \rangle$ for the polymer skeleton and water decrease with increasing
245 temperature and moisture content. In terms of absolute value, the local stiffness of polymer,

246 ranging from 3.0~7.4 10^4 K nm^{-2}, is around 10 times higher than that of water, ranging from
247 0.13~0.83 10^4 K nm^{-2}. This indicates that the stiffness of the hydrated uLGN system is
248 dominated by the stiffness of the polymer chains rather than by the stiffness of the adsorbed
249 water. In fact, the local stiffness of the polymer skeleton (Figure 3a) resembles the overall
250 stiffness of the composite material (Figure 2b), which will be further supported by the correlation
251 analysis in the following sections.

252 3.3 Link between microscopic and macroscopic results

253 In this section, we derive a relationship between the local stiffness $T/\langle u^2 \rangle$ at the microscale
254 and the macroscopic bulk modulus *K*. The bulk modulus *K* refers to the isothermal bulk modulus
255 K_T unless otherwise stated. The time scale studied in this section is in the order of several pico-
256 seconds, therefore the material is assumed to behave elastically (no time effects). The thermal
257 energy, i.e. the translational kinetic energy, of a chain segment equals $\frac{3}{2}k_B T$. If we assume that
258 this chain segment is confined to its equilibrium location by a harmonic spring, the energy of the
259 chain segment movement can be expressed as $k\langle u^2 \rangle$, where k stands for an assumed local spring
260 constant. The maximum potential energy stored in the spring should equal the kinetic energy of
261 the segment:

$$\frac{1}{2}k\langle u^2 \rangle \cong \frac{3}{2}k_B T \tag{4}$$

262 The intrinsic vibration frequency of a harmonic spring is $\omega_0 = \sqrt{k/a\lambda}$, where a is the size of
263 the segment and λ the line density of the polymer chain. Therefore, the wave speed in the
264 material is $c = \omega_0 a$ and we have:

$$c = \omega_0 a = \sqrt{ka/\lambda} \tag{5}$$

The longitudinal wave speed in the material is related to the adiabatic bulk modulus K_s (here we assume $K_s \cong K_T$, which holds for a number of solid materials[42]), the shear modulus G and the density of the material $\rho = \lambda a/a^3$:

$$c = \sqrt{\frac{K_s + \frac{4}{3}G}{\rho}} \tag{6}$$

For an isotropic material, the bulk and shear moduli are related by Poisson's ratio through:

$$G = \frac{3}{2}\frac{K(1-2\nu)}{1+\nu} \tag{7}$$

Combining all these equations we find that the bulk modulus of the dry polymer can be predicted from the local stiffness $T/\langle u^2 \rangle$ by:

$$K = \frac{1+\nu}{1-\nu}\frac{k_B T}{a\langle u^2 \rangle} \tag{8}$$

This equation shows that the bulk modulus at the macroscale is directly related to the amplitude of segmental motion $\langle u^2 \rangle$ or local stiffness $T/\langle u^2 \rangle$ at microscale.

Further, the Young's and shear moduli can be derived for an isotropic material from bulk modulus and Poisson's ratio:

$$E = \frac{3(1+\nu)(1-2\nu)}{1-\nu}\frac{k_B T}{a\langle u^2 \rangle} \quad \text{and} \quad G = \frac{3}{2}\frac{1-2\nu}{1-\nu}\frac{k_B T}{a\langle u^2 \rangle} \tag{9}$$

The eq. (8 and eq. (9) are strikingly simple, considering that only two assumptions, i.e. harmonic vibration and isotropy, are introduced. The relation between the amplitude of segmental motion $\langle u^2 \rangle$ and shear or Young's moduli was shown in,[43] but in this study explicit equations are provided for bulk, Young's and shear moduli as functions of $\langle u^2 \rangle$.

Using eq. (8), the bulk modulus of the dry polymer as a function of temperature can be predicted knowing the local stiffness $T/\langle u^2 \rangle$ at microscale. Here the chain segment is defined as a lignin monomer. As 500 monomers occupy a volume of around 104 nm^3, and given that $500 *$

$a^3 = 104\ \mathrm{nm}^3$, therefore the size of the chain segment is on average $a \sim 0.59$ nm. We remark that there is no strict definition of chain segments and other definitions may give different values of chain segment size. For most of the polymers, the Poisson ratio varies between $0.35 < \nu < 0.45$. A standalone MD test shows that, at 300 K and *m*=0%, the Poisson's ratio of pure uLGN is ~0.37, in accordance with experimental estimation.[44] Figure 4a is the correlation plot of the measured bulk moduli and the local stiffness of the polymer skeleton. The circles denote the average values of the three repetition tests, and the error bars denote the standard deviation. The color of the circles gradually changes from black to red denoting the increase in temperature. The color of the edges of the circles changes from black to blue denoting the increase in moisture content. The Pearson correlation coefficient of 0.96 indicates that $T/\langle u^2 \rangle$ can serve as an indicator for the macroscopic stiffness of the material. We note again that the $\langle u^2 \rangle$ can be measured by neutron scattering experiments,[40] meaning that eq. (8 and eq. (9) might be examined by future experimental studies. Though it is known that MD does not reproduce a heating rate equivalent to the experimental one, the correlation between local stiffness and macroscopic stiffness of material is sound because the $\langle u^2 \rangle$ and bulk moduli are measured using the same heating protocol.

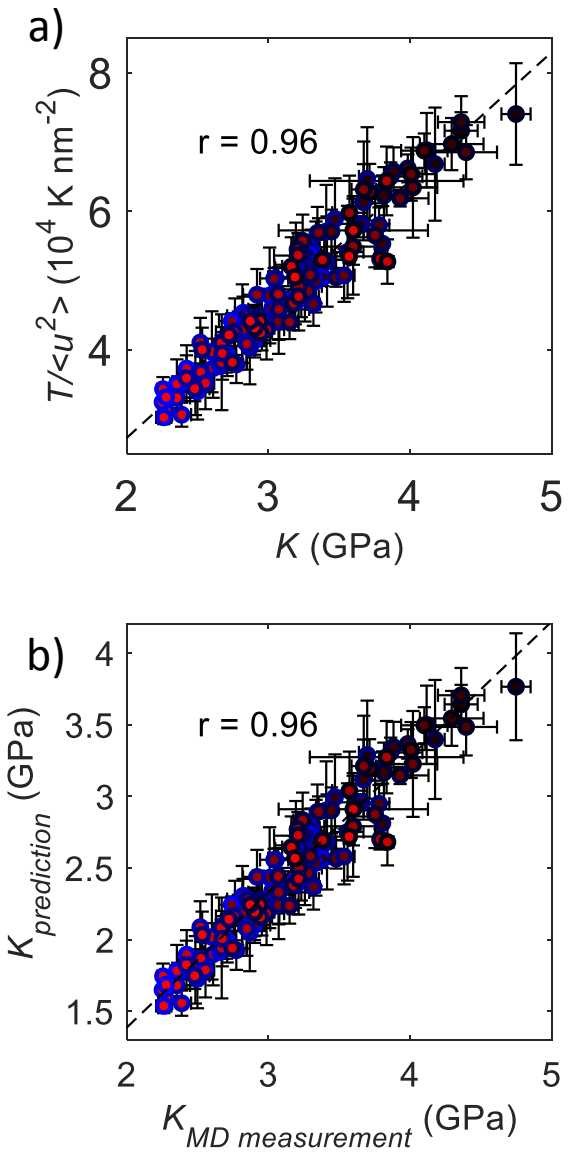

298

299 **Figure 4**. **a**) Correlation plot of local stiffness and the measured bulk moduli. The error bar
300 indicates the standard deviation of the repetition samples. The Pearson correlation coefficient is
301 0.96. **b**) Comparison of the bulk moduli by MD measurement and predicted through the eq. (8).
302 In both figures, marker face color changes from black to red denoting the rise of temperature,
303 and the marker edge color changes from black to blue denoting the rise of moisture content.

304 The local stiffness can be used to predict the stiffness of material using eq. (8). As shown in
305 Figure 4b, the prediction agrees well with MD measurement though the absolute values of

prediction are lower than the measurement. The difference between the MD measurement and the prediction may be attributed to the simplifications made in the derivation of eq. (8), such as assuming elasticity, isotropy and homogeneity, the validity of harmonic confinement assumption, the definition of the chain segment size and the accuracy of the method of bulk moduli measurement. To what extent the idealization assumptions affect the predicting power of eq. (8 might be the topic of future investigations.

As suggested by the form of local stiffness, i.e. $T/\langle u^2 \rangle$, moisture content and temperature influence this mechanical property in different ways. Temperature influencing both T and $\langle u^2 \rangle$, however, moisture content altering only $\langle u^2 \rangle$. Though phenomenologically heat and moisture both induce the macroscopic weakening of material, they impact the molecular mechanics differently.

We can also derive a relation between thermal expansion and local stiffness of the material. In Gruneisen theory,[45,46] based on the existence of an asymmetrical potential energy curve in terms of the distance between atoms, a simple relationship between thermal expansion coefficient and bulk modulus at the macroscale is derived:

$$\alpha = \frac{\gamma_G C_V}{VK} \tag{10}$$

where α, γ_G, C_V, V, K are the volumetric thermal expansion coefficient, Gruneisen parameter (defined as the rate of change of vibrational frequency with expansion), specific heat under constant volume, volume and isothermal bulk modulus, respectively. The Gruneisen theory was originally developed for crystals, however, since we see our systems as chain segments moving around their equilibrated location, it is reasonable to extend the theory to our material. The thermal expansion coefficient α is related to thermal strain $\varepsilon_V = \alpha \mathrm{d}T$. Combining eq. (8) and eq. (10), we find a relation between volumetric thermal strain ε_V and the local stiffness $T/\langle u^2 \rangle$:

$$\varepsilon_V = \frac{1-\nu}{1+\nu}\frac{\gamma_G C_V a\langle u^2\rangle}{V k_B T} \quad (11)$$

This equation shows that the thermal strain increases with the decrease of local stiffness of the material, which depends on both temperature and moisture content. eq. (11 also shows that several other material properties, including Poisson's ratio, Gruneisen parameter, heat capacity, and temperature, determine the thermal expansion of the material. How these material properties are related to each other and a further deduction of eq. (11 into a simpler form can be a future research topic.

3.4 Discussion: Beyond the similarity of heat and moisture

We have shown above that both heat and moisture have a similar effect of expanding/swelling and weakening the material. We also showed that the hygric swelling, thermal expansion and mechanical weakening are all related to the increase of the amplitude of segmental motion on the microscale. In this section, we discuss however the differences between the effects of heat and moisture, beyond their similarity.

3.4.1 Free straining - the difference between the impacts of moisture and heat

We use the data of the free strain $\epsilon_V(m,T)$ dependent on temperature T and moisture content m in Figure 2a to study the combined effect of heat and moisture. To do so, we introduce three different models, and the results of these models are shown in Table 1, where we used the sum of squared errors (SSE) to evaluate the quality of the model. A first model, called the "first-order independent model" assumes that the free strain is linearly correlated with temperature and moisture content, where independent refers to the fact that the contributions of heat and moisture are additive. In a second model, second-order terms in temperature and moisture content are added, called the "second-order independent model". Finally, in the coupled model a coupling term in temperature and moisture content $m*T$ is added to the first-order independent model.

Comparing the SSE of the different models, we observe that the coupling model provides by far the best results, indicating that the coupling between temperature and moisture content is essential in describing the heat-moisture dependence of free strain. This coupling effect between heat and moisture is a first indication that both factors are not just additive, but that there is an interaction between the two factors.

We already have shown that heat facilitates the segmental motions of the polymer chains. Moisture is known to reside as water molecules in between the polymer chains and to interact with the intermolecular interactions between the polymer chains leading to a weakening of the material. As an example of such intermolecular actions, Figure 5 gives the density of the polymer-polymer hydrogen bonds as a function of temperature and moisture content. We observe at the low moisture content ($m<0.1$) a sharp decrease in the number of hydrogen bonds indicating the breakage of hydrogen bonds between the chains, which are replaced by water-polymer hydrogen bonds, leading to a weakening of the material. This weakening of the material by intermolecular interactions of the water molecules in between the polymer chains (breaking of polymer-polymer hydrogen bonds) will, in turn, facilitate lowering the local stiffness and, as such, water molecules in between the chains may be seen as an activator of segmental motions of the chains. This means that the fundamental mechanisms of heat and moisture are different, where moisture has to be seen as an activator, while heat is a direct cause for the segmental motions. This will be further elaborated in the next section.

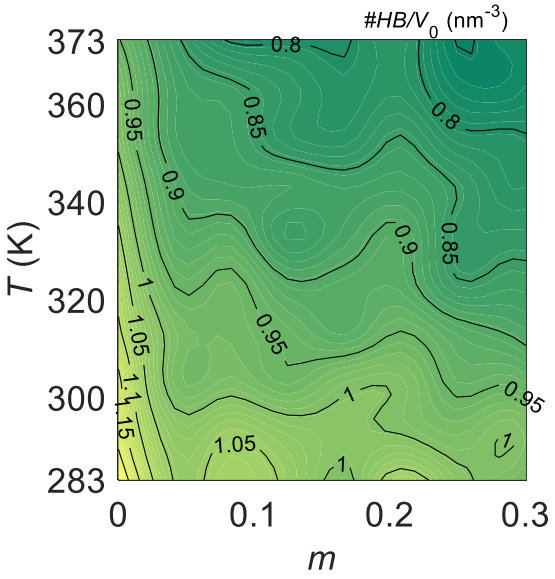

Figure 5. Density of polymer-polymer hydrogen bonds as a function of temperature and moisture content. Units are in nm^{-3}.

Type of model	Fitting of $\epsilon_V(m,T)$	SSE
First order independent model	$1.2m\ -7.6\mathrm{E}^{-4}T\ -0.24$	0.0075
2nd order independent model	$1.2m-\ 4.3\mathrm{E}^{-4}T+0.055m^2+1.8\mathrm{E}^{-6}T^2-0.048$	0.0071
coupling model	$0.72m+3.7\mathrm{E}^{-4}T+1.4\mathrm{E}^{-3}mT-0.12$	0.0011

Table 1. Different models for free strain as a function of temperature and moisture content.

3.4.2 Primary and secondary bond energy – different impacts of moisture and heat

As shown in Figure 2a, uLGN shows an increasing free strain upon increasing temperature, indicating the important role of energetic aspects in the material when being heated. Moreover, as shown in the last sections, the polymer dominates the stiffness of the composite material. Therefore, it is important to analyze the energetic aspects of the uLGN polymer skeleton when the temperature and moisture content increases. The energy terms are obtained through the calculation of potential energy of the polymer skeleton, where the systems consist only of polymer chains after removing all the water molecules from the MD trajectories.

The potential energy of the polymer skeleton consists of two parts: the primary and the secondary bond energy. The primary bond energy includes all the chemical-bond related energies or the so-called "bonded interaction energy" in MD, i.e. bond energy, angle energy, dihedral energy. The secondary bond energy includes all the intermolecular interaction energies or the so-called "non-bonded interaction energy" in MD, i.e. vdW and Coulombic interaction energy. The primary and secondary bond energies of polymer skeleton are shown in Figure 6a and Figure 6b, respectively, where higher and lower values are denoted by yellow and green colors. We note that an increase in potential energy indicates a weakening of the interactions. As shown in Figure 6a, the primary bond energy of polymer skeleton increases mainly with temperature. The contour lines are almost horizontal, indicating an almost negligible influence of moisture content on primary bond energy.

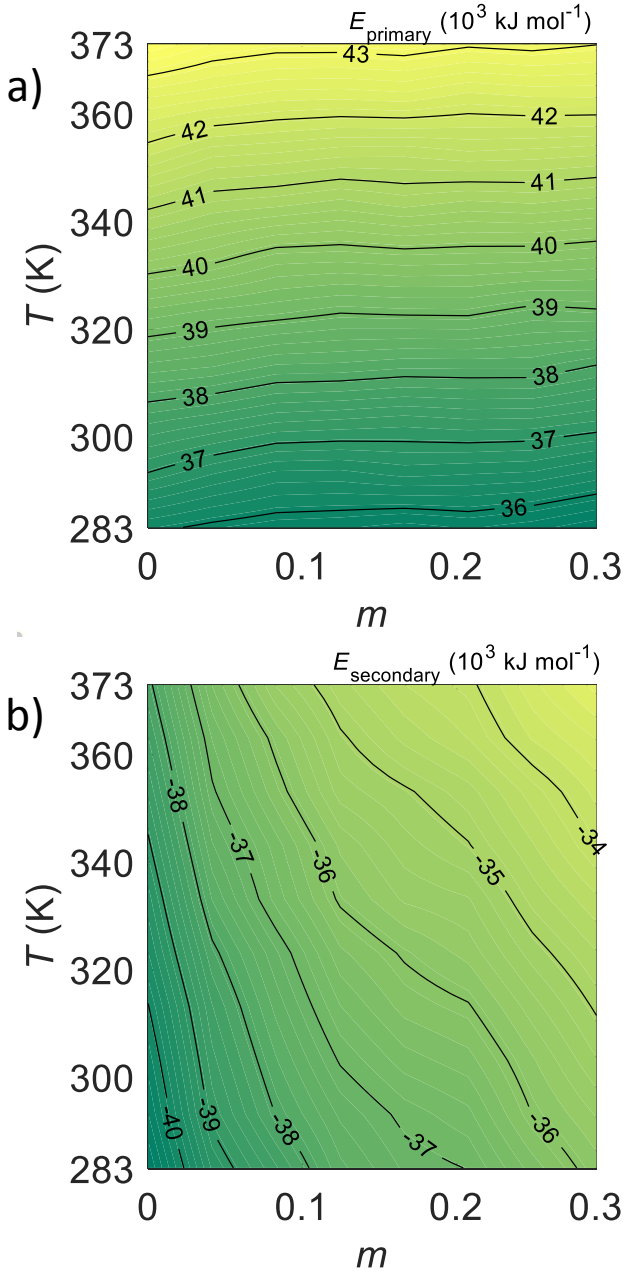

392

393 **Figure 6.** Potential energy of polymer skeleton: **a**) primary bond energy; **b**) secondary bond
394 energy. The unit of the numbers on the contour lines is 10^3 kJ mol^{-1}.

395 Figure 6b shows the secondary bond energy. We observe that moisture strongly influences the
396 secondary bond energy. The density contour lines of secondary bond energy get looser when
397 moisture content increases, indicating that the influence of moisture is getting weaker as

hydration proceeds. This means that the first adsorbed water molecules have a more important impact on the potential energy, as indicated with the smaller spacing between the counter lines. The temperature also influences the secondary bond energy, but to a less extent than the moisture content, while moisture has only a negligible effect on primary bond energy. This implies that water molecules intervene only with intermolecular interactions, e.g. hydrogen bonds, and can hardly affect chemical bond interactions. This agrees with the former report that water relaxes the charged assemblies by interrupting the attraction between oppositely charged groups of the polymers.[47]

Although some similarities between the impact of heat and moisture on free strain and stiffness are observed, in line with the time-temperature-moisture superposition principle proposed by various experimental studies,[1–6] the effects of heat and moisture have different origins. Heat affects both primary and secondary bonds, while moisture only alters secondary bonds, which is the fundamental difference between heat and moisture effects. Considering the important role of primary and secondary bonds on the stiffness of material,[48] our findings may have important implications. To mention one example, for thermosetting polymers, where chains are cross-linked into networks and primary bonds play the dominant role, excessive heat will cause the severance of the primary bonds and consequently weakening,[49] however, the impact of moisture might be limited, which is to be confirmed by future studies.

4. Conclusion

To address the fundamental issue of heat and moisture effects on polymers, this study investigates the prototypical lignin polymer at various temperature and moisture levels using molecular dynamics simulations. In line with previous reports, thermal expansion, hygric swelling and weakening of material occur concomitantly with the increment of temperature and moisture content. The detailed analysis suggests the important role of the coupling between heat

and moisture for the hygric swelling of lignin polymer. To explain the weakening effect, a quantity called local stiffness $T/\langle u^2 \rangle$ is introduced. Under the assumptions of harmonic vibration and isotropy, an equation relating microscopic segmental motions $\langle u^2 \rangle$ to macroscopic modulus is proposed. This equation allows one to theoretically predict the bulk moduli of material, which are in good agreement with the measurement, supporting that the local stiffness is a good indicator for macroscopic local stiffness. Combined with Gruneisen theory, the thermal expansion is shown to be also related to the local stiffness. The energetic analysis of polymer skeleton shows that, while secondary bonds are influenced by both heat and moisture, the primary bonds are affected by heat alone. This indicates the fundamental difference between moisture and heat, the influences of which have long been assumed to be similar, offering a different view of the so-called time-temperature-moisture superposition principle, based on the molecular level inspection.

AUTHOR INFORMATION

Corresponding Author

*E-mail: chi.zhang@empa.ch

Funding Sources

The authors acknowledge the support of the Swiss National Science Foundation (SNSF) grant No. 162957.

Notes

The authors declare no competing financial interest.

444 REFERENCES

445 (1) Emri, I.; Pavsek, V. On the Influence of Moisture on the Mechanical Properties of
446 Polymers. *Met. forum* **1992**, *16* (2).
447 (2) Patankar, K. A.; Dillard, D. A.; Case, S. W.; Ellis, M. W.; Lai, Y.-H.; Budinski, M. K.;
448 Gittleman, C. S. Hygrothermal Characterization of the Viscoelastic Properties of Gore-
449 Select® 57 Proton Exchange Membrane. *Mech. Time-Dependent Mater.* **2008**, *12* (3),
450 221–236. https://doi.org/10.1007/s11043-008-9059-4.
451 (3) Fabre, V.; Quandalle, G.; Billon, N.; Cantournet, S. Time-Temperature-Water Content
452 Equivalence on Dynamic Mechanical Response of Polyamide 6,6. *Polymer (Guildf).* **2018**,
453 *137*, 22–29. https://doi.org/10.1016/j.polymer.2017.10.067.
454 (4) Onogi, S.; Sasaguri, K.; Adachi, T.; Ogihara, S. Time–Humidity Superposition in Some
455 Crystalline Polymers. *J. Polym. Sci.* **1962**, *58* (166), 1–17.
456 https://doi.org/10.1002/pol.1962.1205816601.
457 (5) St. Lawrence, S.; Willett, J. L.; Carriere, C. J. *Effect of Moisture on the Tensile Properties*
458 *of Poly(Hydroxy Ester Ether)*; 2001; Vol. 42. https://doi.org/10.1016/S0032-
459 3861(00)00836-3.
460 (6) Silberstein, M. N.; Pillai, P. V.; Boyce, M. C. Biaxial Elastic–Viscoplastic Behavior of
461 Nafion Membranes. *Polymer (Guildf).* **2011**, *52* (2), 529–539.
462 https://doi.org/10.1016/j.polymer.2010.11.032.
463 (7) Suarez-Martinez, P. C.; Batys, P.; Sammalkorpi, M.; Lutkenhaus, J. L. Time–Temperature
464 and Time–Water Superposition Principles Applied to Poly(Allylamine)/Poly(Acrylic
465 Acid) Complexes. *Macromolecules* **2019**, *52* (8), 3066–3074.
466 https://doi.org/10.1021/acs.macromol.8b02512.
467 (8) Chaléat, C. M.; Michel-Amadry, G.; Halley, P. J.; Truss, R. W. Properties of a Plasticised
468 Starch Blend – Part 2: Influence of Strain Rate, Temperature and Moisture on the Tensile
469 Yield Behaviour. *Carbohydr. Polym.* **2008**, *74* (3), 366–371.
470 https://doi.org/10.1016/j.carbpol.2008.03.002.
471 (9) Williams, M. L.; Landel, R. F.; Ferry, J. D. The Temperature Dependence of Relaxation
472 Mechanisms in Amorphous Polymers and Other Glass-Forming Liquids. *J. Am. Chem.*
473 *Soc.* **1955**, *77* (14), 3701–3707. https://doi.org/10.1021/ja01619a008.
474 (10) Harper, B. D.; Rao, J. M.; Kenner, V. H.; Popelar, C. H. Hygrothermal Effects upon Stress
475 Relaxation in a Polyimide Film. *J. Electron. Mater.* **1997**, *26* (7), 798–804.
476 https://doi.org/10.1007/s11664-997-0254-x.
477 (11) Parodi, E.; Peters, G. W. M.; Govaert, L. E. Prediction of Plasticity-Controlled Failure in
478 Polyamide 6: Influence of Temperature and Relative Humidity. *J. Appl. Polym. Sci.* **2018**,
479 *135* (11), 45942. https://doi.org/10.1002/app.45942.
480 (12) Valentin, D.; Paray, F.; Guetta, B. The Hygrothermal Behaviour of Glass Fibre Reinforced
481 Pa66 Composites: A Study of the Effect of Water Absorption on Their Mechanical
482 Properties. *J. Mater. Sci.* **1987**, *22* (1), 46–56. https://doi.org/10.1007/BF01160550.
483 (13) Petridis, L.; Smith, J. C. A Molecular Mechanics Force Field for Lignin. *J. Comput.*
484 *Chem.* **2009**, *30* (3), 457–467. https://doi.org/10.1002/jcc.21075.
485 (14) Petridis, L.; Schulz, R.; Smith, J. C. Simulation Analysis of the Temperature Dependence
486 of Lignin Structure and Dynamics. *J. Am. Chem. Soc.* **2011**, *133* (50), 20277–20287.
487 https://doi.org/10.1021/ja206839u.
488 (15) Vural, D.; Gainaru, C.; O'Neill, H.; Pu, Y.; Smith, M. D.; Parks, J. M.; Pingali, S. V.;

Mamontov, E.; Davison, B. H.; Sokolov, A. P.; et al. Impact of Hydration and Temperature History on the Structure and Dynamics of Lignin. *Green Chem.* **2018**, *20* (7), 1602–1611. https://doi.org/10.1039/C7GC03796A.

(16) Jin, K.; Qin, Z.; Buehler, M. J. Molecular Deformation Mechanisms of the Wood Cell Wall Material. *J. Mech. Behav. Biomed. Mater.* **2015**, *42*, 198–206. https://doi.org/10.1016/j.jmbbm.2014.11.010.

(17) Beste, A. ReaxFF Study of the Oxidation of Lignin Model Compounds for the Most Common Linkages in Softwood in View of Carbon Fiber Production. *J. Phys. Chem. A* **2014**, *118* (5), 803–814. https://doi.org/10.1021/jp410454q.

(18) Xin, D.; Han, Q. Investigation of Moisture Diffusion in Cross-Linked Epoxy Moulding Compound by Molecular Dynamics Simulation. *Mol. Simul.* **2013**, *39* (4), 322–329. https://doi.org/10.1080/08927022.2012.725204.

(19) Vural, D.; Smith, J. C.; Petridis, L. Dynamics of the Lignin Glass Transition. *Phys. Chem. Chem. Phys.* **2018**, *20* (31), 20504–20512. https://doi.org/10.1039/C8CP03144D.

(20) Dorrestijn, E.; Laarhoven, L. J. J.; Arends, I. W. C. E.; Mulder, P. The Occurrence and Reactivity of Phenoxyl Linkages in Lignin and Low Rank Coal. *J. Anal. Appl. Pyrolysis* **2000**, *54* (1–2), 153–192. https://doi.org/10.1016/S0165-2370(99)00082-0.

(21) Pettersen, R. C. The Chemical Composition of Wood; 1984; pp 57–126. https://doi.org/10.1021/ba-1984-0207.ch002.

(22) Abraham, M. J.; Murtola, T.; Schulz, R.; Páll, S.; Smith, J. C.; Hess, B.; Lindah, E. Gromacs: High Performance Molecular Simulations through Multi-Level Parallelism from Laptops to Supercomputers. *SoftwareX* **2015**, *1–2*, 19–25. https://doi.org/10.1016/j.softx.2015.06.001.

(23) Oostenbrink, C.; Villa, A.; Mark, A. E.; Van Gunsteren, W. F. A Biomolecular Force Field Based on the Free Enthalpy of Hydration and Solvation: The GROMOS Force-Field Parameter Sets 53A5 and 53A6. *J. Comput. Chem.* **2004**, *25* (13), 1656–1676. https://doi.org/10.1002/jcc.20090.

(24) Malde, A. K.; Zuo, L.; Breeze, M.; Stroet, M.; Poger, D.; Nair, P. C.; Oostenbrink, C.; Mark, A. E. An Automated Force Field Topology Builder (ATB) and Repository: Version 1.0. *J. Chem. Theory Comput.* **2011**, *7* (12), 4026–4037. https://doi.org/10.1021/ct200196m.

(25) Canzar, S.; El-Kebir, M.; Pool, R.; Elbassioni, K.; Malde, A. K.; Mark, A. E.; Geerke, D. P.; Stougie, L.; Klau, G. W. Charge Group Partitioning in Biomolecular Simulation. *J. Comput. Biol.* **2013**, *20* (3), 188–198. https://doi.org/10.1089/cmb.2012.0239.

(26) Koziara, K. B.; Stroet, M.; Malde, A. K.; Mark, A. E. Testing and Validation of the Automated Topology Builder (ATB) Version 2.0: Prediction of Hydration Free Enthalpies. *J. Comput. Aided. Mol. Des.* **2014**, *28* (3), 221–233. https://doi.org/10.1007/s10822-014-9713-7.

(27) Terashima, N.; Kitano, K.; Kojima, M.; Yoshida, M.; Yamamoto, H.; Westermark, U. Nanostructural Assembly of Cellulose, Hemicellulose, and Lignin in the Middle Layer of Secondary Wall of Ginkgo Tracheid. *J. Wood Sci.* **2009**, *55* (6), 409–416. https://doi.org/10.1007/s10086-009-1049-x.

(28) Jorgensen, W. L.; Jenson, C. Temperature Dependence of TIP3P, SPC, and TIP4P Water from NPT Monte Carlo Simulations: Seeking Temperatures of Maximum Density. *J. Comput. Chem.* **1998**, *19* (10), 1179–1186. https://doi.org/10.1002/(SICI)1096-987X(19980730)19:10<1179::AID-JCC6>3.0.CO;2-J.

(29) Yang, H.; Yan, R.; Chen, H.; Zheng, C.; Lee, D. H.; Liang, D. T. In-Depth Investigation of Biomass Pyrolysis Based on Three Major Components: Hemicellulose, Cellulose and Lignin. *Energy & Fuels* **2006**, *20* (1), 388–393. https://doi.org/10.1021/ef0580117.
(30) Jackson, C. L.; McKenna, G. B. The Melting Behavior of Organic Materials Confined in Porous Solids. *J. Chem. Phys.* **1990**, *93* (12), 9002–9011. https://doi.org/10.1063/1.459240.
(31) Roduner, E. Thermodynamics of Finite Size Systems. In *Nanoscopic Materials*; Royal Society of Chemistry: Cambridge; pp 119–162. https://doi.org/10.1039/9781847557636-00119.
(32) Kulasinski, K.; Keten, S.; Churakov, S. V.; Guyer, R.; Carmeliet, J.; Derome, D. Molecular Mechanism of Moisture-Induced Transition in Amorphous Cellulose. *ACS Macro Lett.* **2014**, *3* (10), 1037–1040. https://doi.org/10.1021/mz500528m.
(33) Luzar, A.; Chandler, D. Structure and Hydrogen Bond Dynamics of Water–Dimethyl Sulfoxide Mixtures by Computer Simulations. *J. Chem. Phys.* **1993**, *98* (10), 8160–8173. https://doi.org/10.1063/1.464521.
(34) Soper, A. K.; Phillips, M. G. A New Determination of the Structure of Water at 25°C. *Chem. Phys.* **1986**, *107* (1), 47–60. https://doi.org/10.1016/0301-0104(86)85058-3.
(35) Teixeira, J.; Bellissent-Funel, M. C. Dynamics of Water Studied by Neutron Scattering. *J. Phys. Condens. Matter* **1990**, *2*. https://doi.org/10.1088/0953-8984/2/S/011.
(36) Riggleman, R. A.; Douglas, J. F.; de Pablo, J. J. Antiplasticization and the Elastic Properties of Glass-Forming Polymer Liquids. *Soft Matter* **2010**, *6* (2), 292–304. https://doi.org/10.1039/B915592A.
(37) van Zanten, J. H.; Rufener, K. P. Brownian Motion in a Single Relaxation Time Maxwell Fluid. *Phys. Rev. E* **2000**, *62* (4), 5389–5396. https://doi.org/10.1103/PhysRevE.62.5389.
(38) Debye, P. Interferenz von Röntgenstrahlen Und Wärmebewegung. *Ann. Phys.* **1913**, *348* (1), 49–92. https://doi.org/10.1002/andp.19133480105.
(39) Waller, I. Zur Frage Der Einwirkung Der Wärmebewegung Auf Die Interferenz von Röntgenstrahlen. *Zeitschrift für Phys.* **1923**, *17* (1), 398–408. https://doi.org/10.1007/BF01328696.
(40) Price, D. L.; Fernandez-Alonso, F. An Introduction to Neutron Scattering; 2013; pp 1–136. https://doi.org/10.1016/B978-0-12-398374-9.00001-2.
(41) Xia, W.; Song, J.; Jeong, C.; Hsu, D. D.; Phelan, F. R.; Douglas, J. F.; Keten, S. Energy-Renormalization for Achieving Temperature Transferable Coarse-Graining of Polymer Dynamics. *Macromolecules* **2017**, *50* (21), 8787–8796. https://doi.org/10.1021/acs.macromol.7b01717.
(42) Grimvall, G. *Thermophysical Properties of Materials*; Elsevier, 1999. https://doi.org/10.1016/B978-0-444-82794-4.X5000-1.
(43) Zaccai, G. How Soft Is a Protein? A Protein Dynamics Force Constant Measured by Neutron Scattering. *Science (80-.).* **2000**, *288* (5471), 1604–1607. https://doi.org/10.1126/science.288.5471.1604.
(44) Salmén, L. Micromechanical Understanding of the Cell-Wall Structure. *Comptes Rendus - Biol.* **2004**, *327* (9–10), 873–880. https://doi.org/10.1016/j.crvi.2004.03.010.
(45) Tabor, D. *Gases, Liquids and Solids: And Other States of Matter*; Cambridge University Press, 1991.
(46) Grüneisen, E. Theorie Des Festen Zustandes Einatomiger Elemente. *Ann. Phys.* **1912**, *344* (12), 257–306. https://doi.org/10.1002/andp.19123441202.

(47) Zhang, Y.; Batys, P.; O'Neal, J. T.; Li, F.; Sammalkorpi, M.; Lutkenhaus, J. L. Molecular Origin of the Glass Transition in Polyelectrolyte Assemblies. *ACS Cent. Sci.* **2018**, *4* (5), 638–644. https://doi.org/10.1021/acscentsci.8b00137.
(48) Soboyejo, W. *Mechanical Properties of Engineered Materials*; 2002. https://doi.org/10.1201/9780203910399.
(49) Callister Jr, W. D. *Materials Science and Engineering - An Introduction (5th Ed.)*; 2000; Vol. 47. https://doi.org/10.1108/acmm.2000.12847aae.001.

Disentangling Heat and Moisture Effects on Biopolymer Mechanics

Chi Zhang[†‡*], *Ali Shomali*[†], *Robert Guyer*[※], *Sinan Keten*[§], *Benoit Coasne*[‖], *Dominique Derome*[‡], *Jan Carmeliet*[†]